J. Inst. Eng. India Ser. B (December 2020) 101(6):677–688
https://doi.org/10.1007/s40031-020-00490-5

ORIGINAL CONTRIBUTION

Adaptive Kalman Filtering Model Predictive Controller Design for Stabilizing and Trajectory Tracking of Inverted Pendulum

Akshaya Kumar Patra[1]

Received: 11 August 2019 / Accepted: 5 September 2020 / Published online: 21 September 2020
© The Institution of Engineers (India) 2020

Abstract The goal of this manuscript is to formulate a Kalman Filtering Model Predictive Controller (KFMPC) for control of cart position, cart velocity, angular position, and angular velocity of pendulum within a stable range under model uncertainties and disturbances. For designing of the KFMPC, a 4th-order linearized structure of the inverted pendulum system is taken. In this strategy, the conventional model predictive controller is re-formulated with a state estimator based on the Kalman filtering strategy to update the control actions. The approval of the updated control execution of KFMPC is built up by comparative outcome examination with other well-known control techniques. The comparative results obviously expose the better action of the proposed strategy to monitor the system outcomes inside the steady range as far as accuracy, robustness, and stability.

Keywords angular position · IPS · State estimator · Laguerre functions · Model predictive control

Introduction

The IPS control problem is of paramount concern among other control problems due to under-actuated, nonlinear, and the non-minimum phase properties as discussed in [1–3]. Also, this IPS finds numerous industry-based applications like rockets, robots, guided missiles, different crane structures, and a Segway or self-balancing vehicles with two wheels as reported in [4]. In the current work, owing to prominent control dynamics relevance, the IPS has been chosen by an adaptive control law after its proper testing and analysis. Around last thirty years, several strategies of control techniques are put forth and verified for AP control of pendulum within the range of stability. In the problems of IPS with measured AP-based variable gains of the controller, the strategies of control like switching PID and time discrete are implemented as explained in [5, 6]. The practical application of the above-mentioned controllers is infeasible owing to limitations like the setting of the optimal gain variable with a lower robust control range and the necessity of the gain setting change according to the variation in the operating conditions. Among several other highlighted optimal control methods applied to limit the AP and AV of a pendulum are Fuzzy [7], LQR [8–10], neurocontrol [11], backstepping control [12], passivity control [13], state feedback control [14], H-infinity control [15], sliding-mode (SM) control [16], fuzzy sliding-mode (FSM) control [17, 18], and BLQG control [19]. Although the AP and AV control of the IPS with improved accuracy by applying the aforementioned control methods has been quite effective, still they fail to deal several constraints and arbitrary changes observed in the pendulum trajectory motion. Irrespective of better performance, these techniques of control are not capable of nullifying the model's uncertainties and disturbances completely. So, based on the concept of model predictive control and Kalman filtering, an innovative hybrid method has been proposed that sets the control variables optimally to achieve enhanced performance along with avoiding the process disturbance $F(t)$ generated sluggish response.

In current work, a hybrid controller named as KFMPC is developed based on the cascade connection of the CMPC

✉ Akshaya Kumar Patra
hiakp@yahoo.com; akshayapatra@soa.ac.in

[1] Department of Electrical, Electronics Engineering, ITER, Siksha 'O'Anusandhan University, Bhubaneswar 751030, Odisha, India

and Kalman filter. This hybrid method provides an improved action of the resulting controller in terms of uncertainty handling ability, robustness, and accuracy. Here, CMPC is modified taking a state estimator as per the Kalman filtering technique, and this novelty in this formulation provides improved results. Hence, the IPS states are evaluated iteratively following the Kalman filtering method so as to achieve increased system performances. Also, the formation of a stabilizing control law is evolved by the use of the Kalman filtering method and has been reported in [20–26]. The KFMPC is applied for controlling pendulum AP to guarantee an enhanced capacity of elimination of high-level noises, improved capacity to deal with uncertainty, increased robustness, high accuracy, and upgraded stability.

The highlights of this article are:

- Development of a SIMULINK model of an IPS.
- Design of a KFMPC to control the AP of the pendulum within the stable range from − 0.05 rad to + 0.05 rad.
- Estimation of the control actions of the KFMPC under huge deviation of process disturbance $F(t)$.
- Comparative investigation to certify the better response of the KFMPC.

The remaining part of the article is outlined as follows. "Problem Formulations" section precisely explains the mathematical details of the IPS that reflects its dynamic features. A detailed control technique formulation and its implementation of the current problem are covered in "Control Algorithms" section. The outcomes of the suggested technique and comparative analysis with other proven control methodologies are presented in "Outcomes and Deliberations" section. The concluding remarks are detailed in "Conclusions" section.

Problem Formulations

System Overview

The IPS with KFMPC is displayed in Fig. 1a. In the present study, the horizontal force $F(t)$ is the disturbance to the process, and $v(t)$ is the sensor noise. The AP information of the pendulum is received by the KFMPC as an input for the generation of the optimal force of control $u(t)$ that helps in the pendulum balance.

Mathematical Model of IPS

Figure 1b illustrates the structure of the cart–pendulum linked to a flexible cart rail having a pole that can swing freely, and one DC motor controls the CP. The nonlinear mathematical model of the IPS based on Newton's law is being developed over here. It is assumed that the CP gets affected by $F(t)$ due to action of the DC motor [27–30]. The mathematical expressions of the IPS dynamics are stated in Eqs. (1) and (2). The variables and standard input data of the IPS are put in Tables 1 and 2, respectively. The mathematical structure of the IPS is formulated in accordance with Eqs. (1) and (2) as presented in Fig. 1c.

$$(M+m)\frac{d^2x(t)}{dt^2} - ml\frac{d^2\theta(t)}{dt^2}\cos\theta(t) + ml\left(\frac{d\theta(t)}{dt}\right)^2\sin\theta(t) + b\frac{dx(t)}{dt} = F(t) \tag{1}$$

$$\left(i+Ml^2\right)\frac{d^2\theta(t)}{dt^2} - mgl\sin\theta(t) = ml\frac{d^2x(t)}{dt^2}\cos\theta(t) \tag{2}$$

Linearization of the Nonlinear System

The nonlinear nominal model (NM) of an IPS is linearized near the operating point for the formulation of KFMPC to monitor the system outcomes within the stable range. The linearization of the non-direct framework elements concerning Eqs. (1) and (2) is established by ignoring the higher-order components such as $\left(\frac{d\theta(t)}{dt}\right)^2$. For linearization of the nonlinear IPS, the dynamic Eqs. (1) and (2) are reduced to Eqs. (3) and (4) based on the stable conditions such as $\theta(t) = 0$, $\frac{d^2\theta(t)}{dt^2} \cong 0$, and $\cos(0) = 1$

$$(M+m)\frac{d^2x(t)}{dt^2} + b\frac{dx(t)}{dt} - ml\frac{d^2\theta(t)}{dt^2} = F(t) \tag{3}$$

$$\left(i+ml^2\right)\frac{d^2\theta(t)}{dt^2} - mgl\theta(t) = ml\frac{d^2x(t)}{dt^2} \tag{4}$$

The TF of the CP and AP of the IPS are stated as [27]:

$$\frac{X(s)}{U(s)} = \frac{\frac{(i+ml^2)s^2-mgl}{\psi}}{s^4 + \frac{b(i+ml^2)}{\psi}s^3 - \frac{(M+m)mgl}{\psi}s^2 - \frac{bmgl}{\psi}s} \tag{5}$$

$$\frac{\theta(s)}{U(s)} = \frac{\frac{ml}{\psi}s}{s^3 + \frac{b(i+ml^2)}{\psi}s^2 - \frac{(M+m)mgl}{\psi}s - \frac{bmgl}{\psi}} \tag{6}$$

where $\psi = [(M+m)(i+Ml^2) - ml^2]$. The linearized equation of the IPS with $F(t)$ and $v(t)$ with respect to Eqs. (5) and (6) is stated as [27]:

$$\left.\begin{aligned}\frac{dx_m(t)}{dt} = \dot{x}_m(t) &= A_m x_m(t) + B_m u(t) + B_d F(t)\\ y(t) &= C_m x_m(t) + D_m u(t) + v(t)\end{aligned}\right\} \tag{7}$$

where $x_m(t)$, $u(t)$, and $y(t)$ are represented as the state variable, control input, and measured output, respectively. The $x_m(t)$ is composed with the AP, CP, AV, and CV. The state-space matrices of the NM of the IPS are denoted as A_m, B_m, C_m, D_m, and B_d. These are derived from the

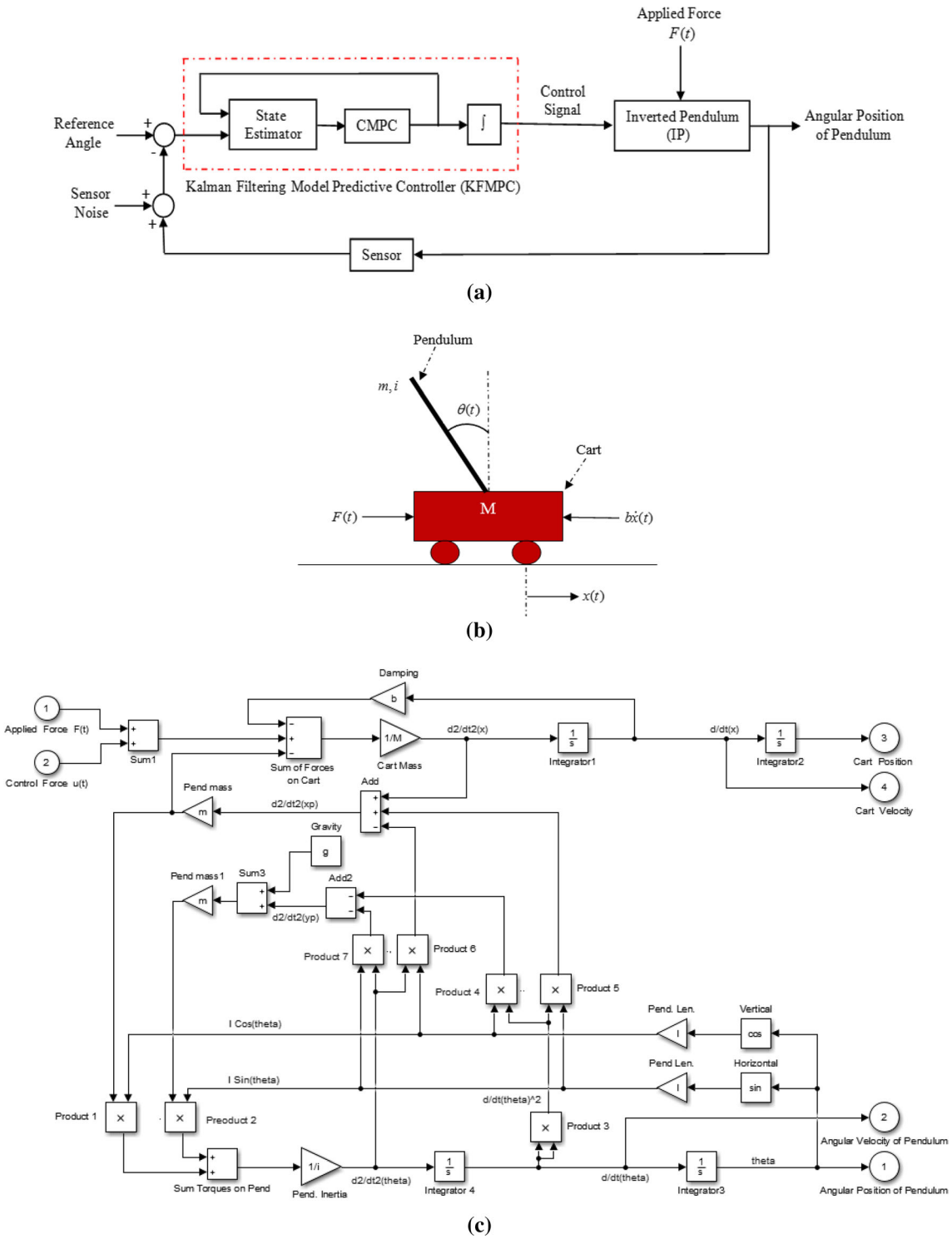

Fig. 1 **a** Closed-loop feedback control of IPS; **b** graphical representation of the IPS; **c** mathematical structure of the nonlinear IPS; and **d** the force $F(t)$ on the IPS at the time of 0.1 s

linearization of the IPS dynamics nearby the reference point. It is discussed in detail in reference [27]. In MATLAB, the keyword "*linmod*" is utilized to assess the state-space matrices on the mathematical structure of IPS as portrayed in Fig. 1c.

Investigation of IPS Activities

There IPS has 4 roots. But only 1 root is locked in right side of the frequency domain. Subsequently, the IPS gets insecure. It desires the formulation of a robust control

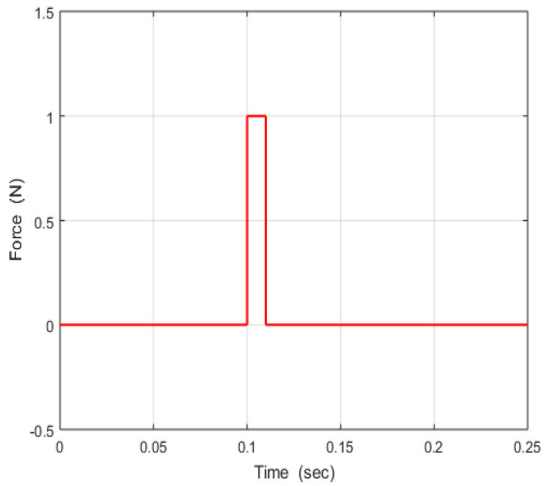

(d)

Fig. 1 continued

Table 1 IPS variables

Symbol	Representation
$F(t)$	Force on the cart in horizontal direction
$b\frac{dx(t)}{dt}$	Force on the cart due to friction
$x(t)$, $\frac{dx(t)}{dt}$, $\frac{d^2x(t)}{dt^2}$	CP, CV, and cart acceleration, respectively
$\theta(t)$, $\frac{d\theta(t)}{dt}$, $\frac{d^2\theta(t)}{dt^2}$	AP, AV, and acceleration of pendulum, respectively

Table 2 IPS specifications

Symbol	Physical meaning	Value
M	Cart mass	0.5 kg
m	Pendulum mass	0.2 kg
i	Inertia	0.3 kg.m^2
g	Acceleration due to gravity	9.8 m/s^2
b	Coefficient of frictional	0.1 N.s/m
l	Length of pendulum	0.3 m

algorithm to update the stability of the IPS by pulling the roots in the direction of the left side of the frequency domain. The open-loop mathematical structure of IPS is portrayed in Fig. 1c. The IPS comprises of 2 inputs and 4 outcomes. The 2-input variables are $u(t)$ and $F(t)$, and CP, CV, AP, and AV are the 4 outcomes of the IPS. Uncontrolled system outcomes are being observed to the use of 1 N impulsive $F(t)$ on the IPS at the time of 1.0 s. Those outcomes are delineated in Fig. 2a–d. Figure 2a–d shows the unstable outcomes in the presence of model uncertainties and disturbances. The unstable nature of the outcomes can be decreased by implementing the appropriate control methods. Right now, AP of the IPS is the most fundamental outcome that should be monitored in a steady range through appropriate control methods, and other 3 outcomes are examined so as to see the motion route.

Control Algorithms

The KFMPC strategy is exhibited in this segment. The IPS activity concerning robustness, accuracy, and stability is examined through the KFMPC. The control features like settling time t_s, steady-state error e_{ss}, peak overshoot O_{Peak}, and peak undershoot U_{Peak} are additionally assessed and inspected with appropriate approval of the KFMPC action.

Design of KFMPC

The linearized structure of the IPS as demonstrated in "Linearization of the nonlinear system" section has been considered for the design of the KFMPC to control the outcomes of the IPS. For achieving an upgraded response and proper execution of control variables of the KFMPC, it is cascaded to the IPS as shown in Fig. 3. In this strategy, system states are recursively estimated through the Kalman filter to upgrade the control execution. The linearized IPS with $v(t)$ and $F(t)$ is framed as signified in Eq. (7), where both $v(t)$ and $w(t)$ are the Gaussian noise, and these are associated as:

$$\left.\begin{aligned} E\{F(t)\} &= 0 \\ E\{v(t)\} &= 0 \end{aligned}\right\} \tag{8}$$

$$E\{F(t)F^T(\tau)\} = Q_2\delta(t-\tau) \tag{9}$$

$$E\{v(t)v^T(\tau)\} = R_2\delta(t-\tau) \tag{10}$$

The $F(t)$ and $v(t)$ are uncorrelated to each other, i.e.,

$$E\{F(t)v^T(\tau)\} = 0 \tag{11}$$

where Q_2 and R_2 are the intensities of the $F(t)$ and $v(t)$, respectively. Figure 3 demonstrates the linearized structure of the IPS with the feedback gain K_{mpc} and Kalman filter gain K_f. The mathematical expressions of K_{mpc} and K_f are clearly mentioned in "Feedback gain K_{mpc} of KFMPC" and "Kalman Filter Gain K_f" sections, respectively. The estimation of the TF of the KFMPC is clearly defined in "TF of the KFMPC" section.

The first differentiation of the control signal $\frac{du(t)}{dt}$ of the proposed KFMPC is represented in Eq. (12).

$$\frac{du(t)}{dt} = \dot{u}(t) = -K_{mpc}\hat{x}_a(t) \tag{12}$$

where K_{mpc} is the feedback gain of the proposed KFMPC, and $\hat{x}_a(t)$ is the estimated state variable of the augmented model (AM) of the IPS. The $\frac{du(t)}{dt}$ is regulated by K_{mpc} with respect to $\hat{x}_a(t)$.

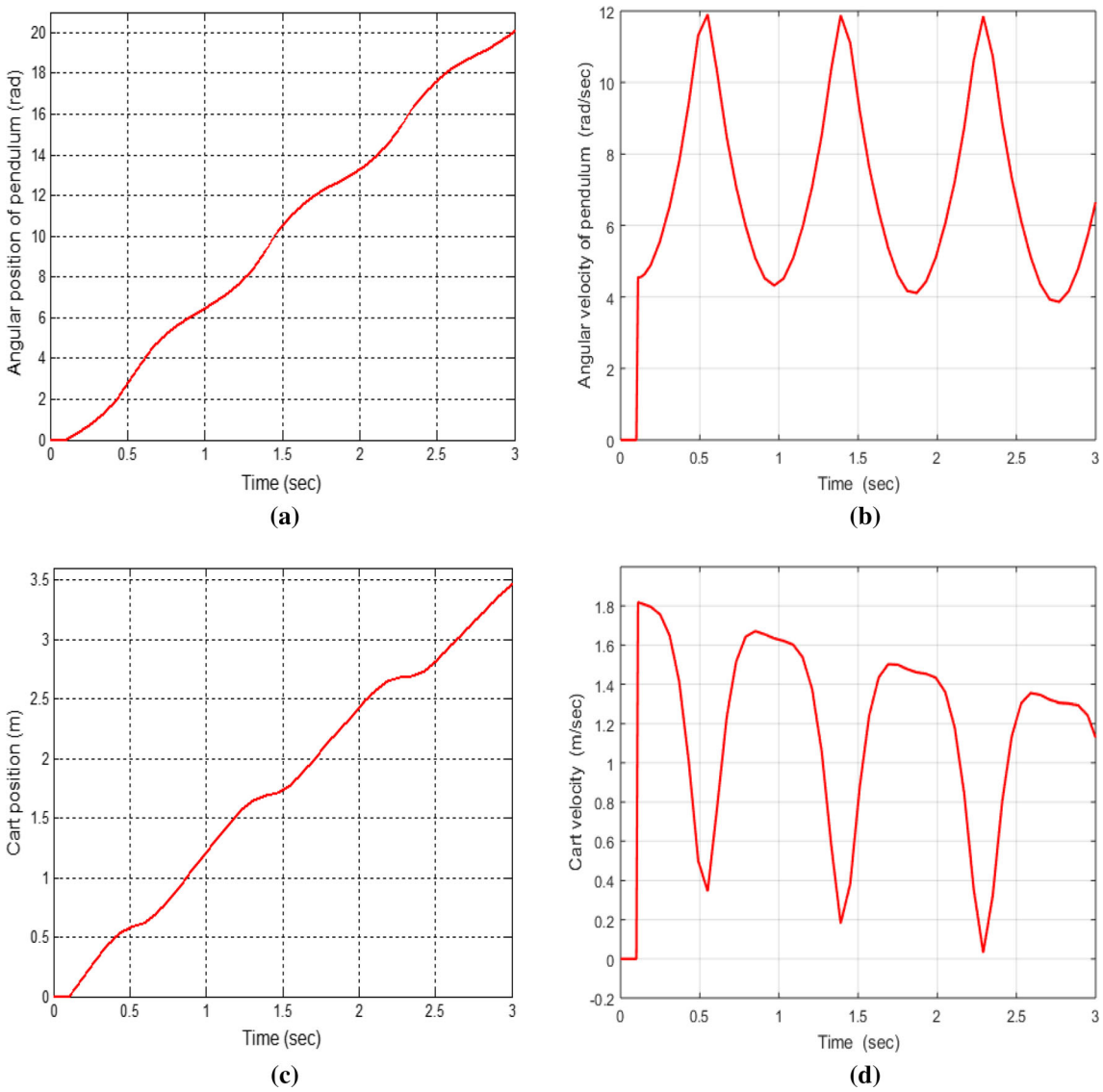

Fig. 2 Outcomes of the open-loop IPS: **a** AP; **c** AV; **c** CP; and **d** CV

Structure of KFMPC Design

The KFMPC is designed based on the receding horizon control (RHC) algorithm. Under this algorithm, one AM is to be formulated based on the NM of a system in such a manner that a first differentiation of the control signal can be embedded through the integrator into the NM of a system to eliminate the any type of noise and disturbance, while maintaining the same output as shown in Fig. 3.

Formulation of AM of IPS: The state-space equation of the NM of the IPS with m inputs and q outputs is stated as:

$$\left.\begin{aligned}\frac{dx_m(t)}{dt} &= A_m x_m(t) + B_m u(t) + B_d F(t)\\ y(t) &= C_m x_m(t) + D_m u(t) + v(t)\end{aligned}\right\} \tag{13}$$

where dimension of $x_m(t)$ is $n_1 \times 1$, and n_1 is the order of the A_m. The dimensions of A_m, B_m, and C_m matrices are $n_1 \times n_1$, $n_1 \times m$, and $q \times n_1$, respectively. Under the RHC algorithm, current data on the NM of IPS are predicted and controlled. It is assumed that $y(t)$ is not affected by the $u(t)$ and during the same moment, D_m is zero in NM of the IPS. For the formulation of AM of an IPS based on Eq. (13), the new state variables are considered as follows:

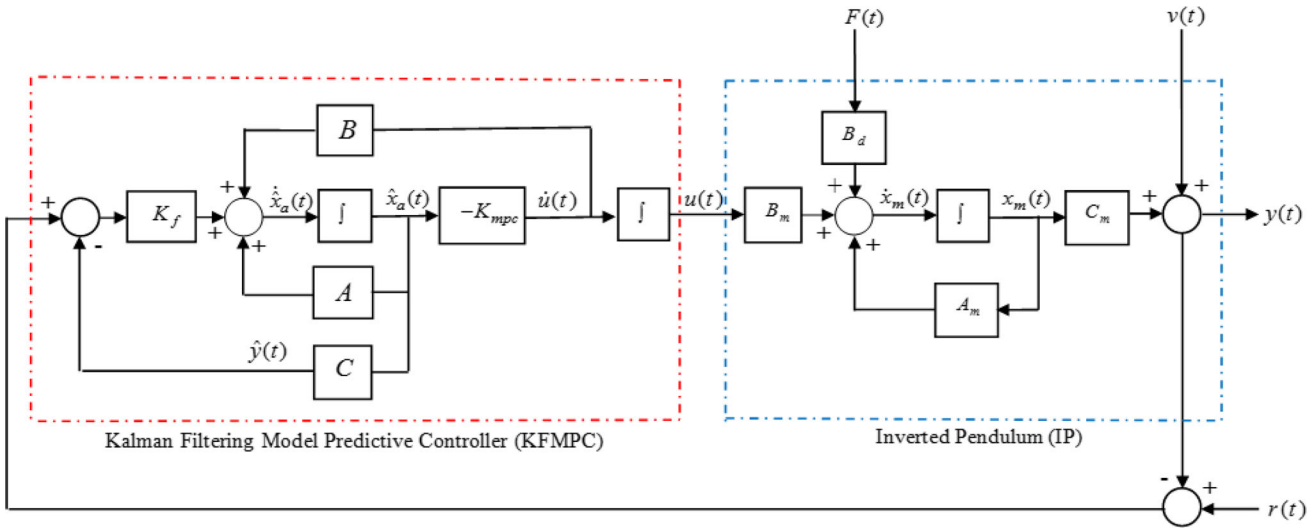

Fig. 3 The structure of IPS with KFMPC in the state-space platform

$$\left.\begin{aligned} z(t) &= \frac{dx_m(t)}{dt} \\ y(t) &= C_m x_m(t) + v(t) \end{aligned}\right\} \tag{14}$$

The state variable of the AM of the IPS $x_a(t)$ is formulated based on Eqs. (13) and (14) as:

$$x_a(t) = \begin{bmatrix} z(t)^T & y(t)^T \end{bmatrix}^T \tag{15}$$

The state-space equation of AM of the IPS is formulated with respect to Eq. (13) as follows [20]:

$$\begin{bmatrix} \frac{dz(t)}{dt} \\ \frac{dy(t)}{dt} \end{bmatrix} = \overbrace{\begin{bmatrix} A_m & o_m^T \\ C_m & o_{q\times q} \end{bmatrix}}^{A} \begin{bmatrix} z(t) \\ y(t) \end{bmatrix} + \overbrace{\begin{bmatrix} B_m \\ o_{q\times m} \end{bmatrix}}^{B} \frac{du(t)}{dt} + \overbrace{\begin{bmatrix} B_d \\ o_{q\times m} \end{bmatrix}}^{G} \frac{dF(t)}{dt} \tag{16}$$

$$y(t) = \underbrace{\begin{bmatrix} o_m & I_{q\times q} \end{bmatrix}}_{C} \begin{bmatrix} z(t) \\ y(t) \end{bmatrix} + v(t) \tag{17}$$

where o_m, $o_{q\times q}$, and $o_{q\times m}$ are the zero matrices with dimensions of $q \times n_1$, $q \times q$, and $q \times m$, respectively. The $I_{q\times q}$ is an identity matrix with dimension of $q \times q$. Equations (16) and (17) can be rewritten as:

$$\left.\begin{aligned} \frac{dx_a(t)}{dt} &= Ax_a(t) + B\frac{du(t)}{dt} + G\frac{dF(t)}{dt} \\ y(t) &= Cx_a(t) + v(t) \end{aligned}\right\} \tag{18}$$

where $x_a(t)$ has two major components such as $\frac{dx_m(t)}{dt}$ and $y(t)$. The dimension of $x_a(t)$ is $n \times 1$, and n is equal to the $n_1 + q$. The state-space matrices of the AM of the IPS are represented as A, B, C, and G. The $\frac{du(t)}{dt}$ is the input to the AM of IPS, and output remains same, which is visualized in Eq. (18).

AM with Deterministic Disturbance When $F(t)$ is deterministic in nature, it is always constant. Under this situation, the first derivative of $F(t)$ with respect to time is zero, which is defined as follows:

$$\frac{dF(t)}{dt} = 0 \tag{19}$$

The state-space equation of AM of IPS with deterministic process disturbance with respect to Eq. (18) is:

$$\left.\begin{aligned} \frac{dx_a(t)}{dt} &= Ax_a(t) + B\frac{du(t)}{dt} \\ y(t) &= Cx_a(t) + v(t) \end{aligned}\right\} \tag{20}$$

where $\frac{dF(t)}{dt}$ is equal to zero.

AM with Stochastic Disturbance When $F(t)$ is stochastic in nature, it is random. It is stated as:

$$F(t) = \int_0^t \varepsilon(\tau)d\tau \tag{21}$$

where $\varepsilon(.)$ is represented as a band-limited, zero mean, and white noise vector. It is defined as:

$$E\left\{\frac{dF(t)}{dt}\right\} = E\{\varepsilon(t)\} = 0 \tag{22}$$

where $E\{\}$ is the expectation function. The state-space equation of AM of IPS with stochastic process disturbance is represented in Eqs. (23) and (24).

Table 3 The control variables

Q_1	R_1	Q_2	R_2
$1000 * C^T * C$	1	0.01	0.0025

$$\begin{bmatrix} \frac{dz(t)}{dt} \\ \frac{dy(t)}{dt} \end{bmatrix} = \overbrace{\begin{bmatrix} A_m & o_m^T \\ C_m & o_{q\times q} \end{bmatrix}}^{A} \begin{bmatrix} z(t) \\ y(t) \end{bmatrix} + \overbrace{\begin{bmatrix} B_m \\ o_{q\times m} \end{bmatrix}}^{B} \frac{du(t)}{dt} + \overbrace{\begin{bmatrix} B_d \\ o_{q\times m} \end{bmatrix}}^{G} \varepsilon(t) \tag{23}$$

$$y(t) = \underbrace{\begin{bmatrix} o_m & I_{q\times q} \end{bmatrix}}_{C} \begin{bmatrix} z(t) \\ y(t) \end{bmatrix} + v(t) \tag{24}$$

where G is a matrix of stochastic process disturbance. When the AM is to be predicted and controlled in the presence of stochastic noise, the effect of that disturbance in expectance on the future state will be zero.

Feedback gain K_{mpc} of KFMPC

The K_{mpc} is assessed concerning the IPS activities for the least value of the objective function j as stated in Eq. (25).

$$j = \int_0^\infty \left[x_a(t)^T Q_1 x_a(t) + \left(\frac{du(t)}{dt} \right)^T R_1 \frac{du(t)}{dt} \right] dt \tag{25}$$

where $Q_1 = C^T q_1 C$. The Q_1, q_1, and R_1 are denoted as the state weighting matrix, the intensity of the Q, and the input weighting matrix, respectively. The K_{mpc} of the KFMPC for the least value of the j is stated as:

$$K_{mpc} = \begin{bmatrix} L_1(0)^T & o_2 & . & . & . & o_m \\ o_1 & L_2(0)^T & . & . & . & o_m \\ . & . & . & & & . \\ . & . & & . & & . \\ . & . & & & . & . \\ o_1 & o_2 & . & . & . & L_m(0)^T \end{bmatrix} \Omega^{-1}\Psi \tag{26}$$

where $o_1, o_2, \ldots, o_m$ are the zero matrices of 1st input, 2nd input, ..., m^{th} input, respectively. All sizes above zero matrices are equal and considered as $q \times n$. The $L_1(0)$, $L_2(0)$, ..., $L_m(0)$ are the initial conditions of 1st input, 2nd input, ..., m^{th} input, respectively. All initial conditions of all inputs are same and considered as:

$$L(0) = \sqrt{2p}[\,1 \quad 1 \quad . \quad . \quad . \quad 1\,]^T \tag{27}$$

It is a column vector and contains N numbers of elements. Here, N represents the number of Laguerre networks [20], and p stands for scaling factor.

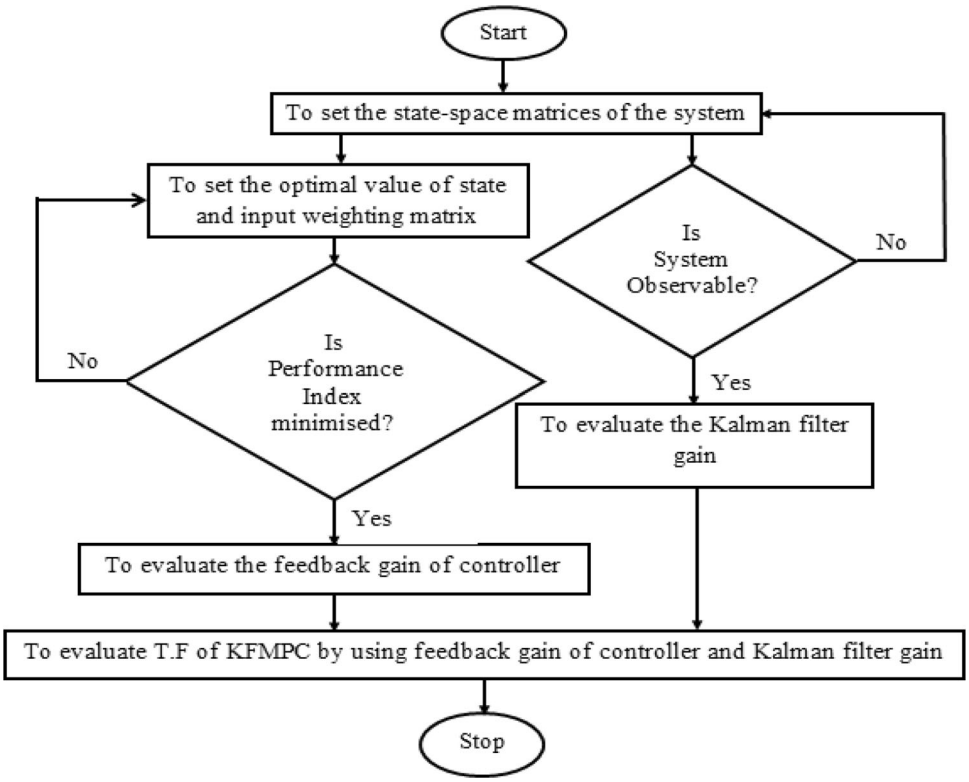

Fig. 4 The flowchart of the KFMPC

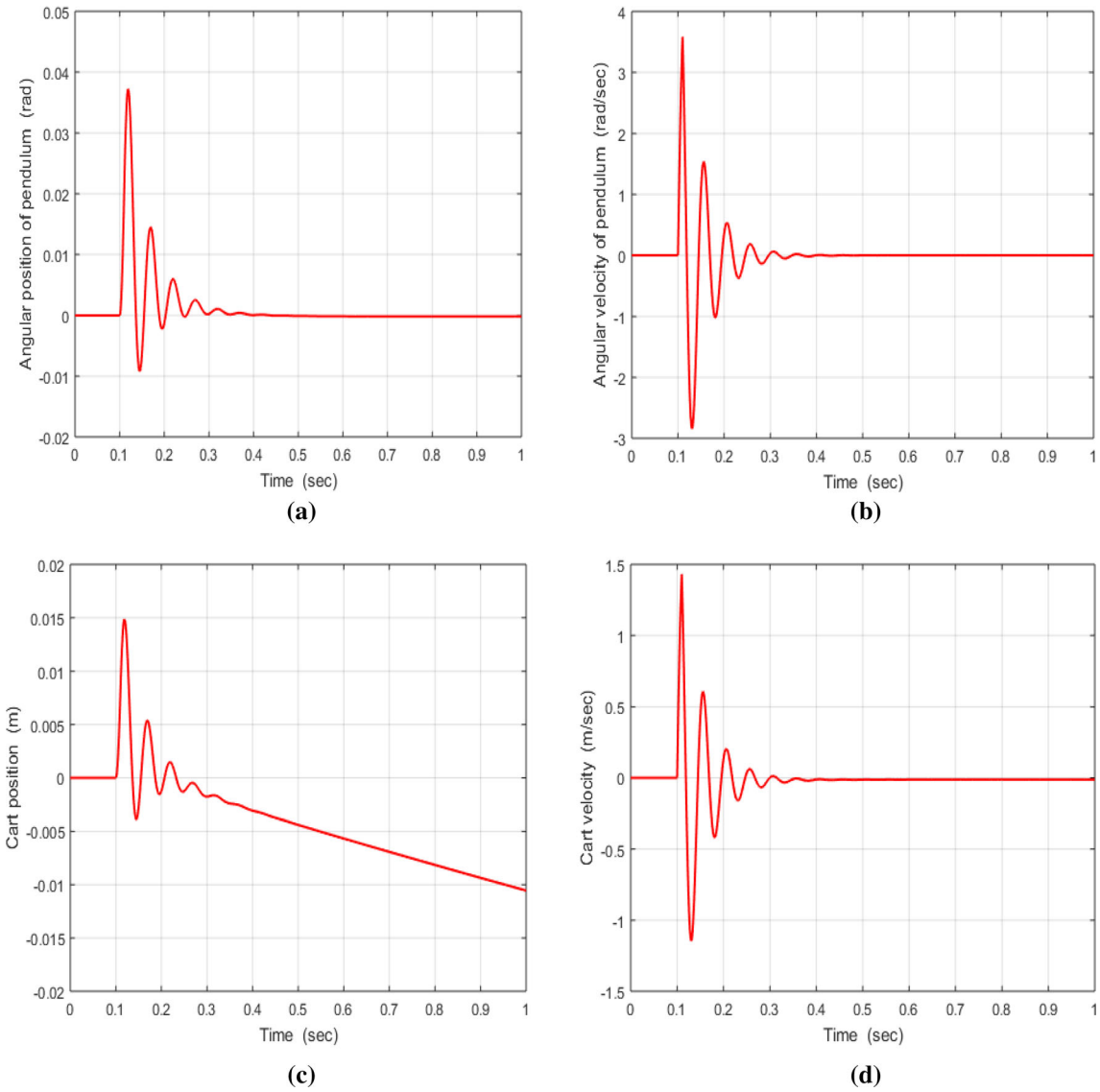

Fig. 5 Outcomes of IPS with KFMPC: **a** AP; **b** AV; **c** CP; and **d** CV

The Ω and Ψ are the constant matrices and defined as in Eq. (28).

$$\left.\begin{aligned}\Omega &= \sum_{k=0}^{M} \varphi(kh) Q \varphi(kh)^T h + R_L \\ \Psi &= \sum_{k=0}^{M} \varphi(kh) Q e^{Akh} h\end{aligned}\right\} \tag{28}$$

where M represents the number of samples and is defined as in Eq. (29).

$$M = \frac{T_p}{h} \tag{29}$$

T_p and h represent the total prediction horizon time and sample interval, respectively, and k varies from zero to M.

The $\varphi(kh)^T$ is a solution of the linear algebraic equation and expressed as:

$$A\varphi(kh)^T - \varphi(kh)^T A_p^T = -BL(kh)^T + e^{Akh} BL(0)^T \tag{30}$$

where $L(kh)$ represents the set of Laguerre functions and is defined in Eq. (31).

$$L(kh) = e^{A_p kh} L(0) \tag{31}$$

where A_p represents the lower triangular matrix with size of $N \times N$ and is given by [20]:

$$A_p = \begin{bmatrix} -p & 0 & . & . & . & 0 \\ -2p & -p & . & . & . & 0 \\ . & & & & & \\ . & & & & & \\ . & & & & & \\ -2p & . & . & . & -2p & -p \end{bmatrix} \tag{32}$$

It contains R_L number of block diagonal matrices with α^{th} blocks as R_α. The R_α can be defined as:

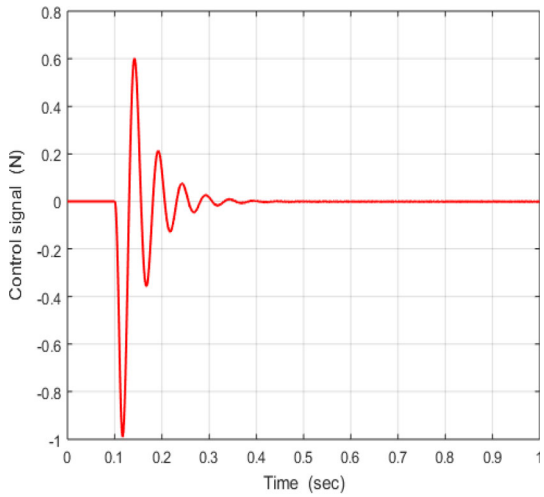

Fig. 6 Control signal $u(t)$ caused by the KFMPC

$$R_\alpha = RI_{N_\alpha \times N_\alpha} \tag{33}$$

where $I_{N_\alpha \times N_\alpha}$ is an unitary matrix with size of $N_\alpha \times N_\alpha$, and α varies from 1 to m.

Kalman Filter Gain K_f

The IPS states are estimated recursively through the Kalman filter to update the system performance. The estimated state-space equation of the IPS is stated as:

$$\left.\begin{aligned} &\frac{d\hat{x}_a(t)}{dt} = \dot{\hat{x}}_a(t) = A\hat{x}_a(t) + B\frac{du(t)}{dt} + K_f[r(t) - y(t) - \hat{y}(t)] \\ &= (A - BK_{mpc} - K_f C_m)\hat{x}_a(t) + K_f[r(t) - y(t)] \\ &\hat{y}(t) = C_m \hat{x}_a(t) \end{aligned}\right\} \tag{34}$$

where $e(t) = [r(t) - y(t)]$, $\hat{y}(t)$ is denoted as the estimated output, and $r(t)$ is denoted as the desired AP of the pendulum. The K_f is computed as [20]:

$$K_f = \prod_f C^T R_2^{-1} \tag{35}$$

where $\prod_f$ is the solution of the Filter Algebraic Riccati Equation (FARE). The FARE is stated as:

$$A\prod_f + \prod_f A^T + GQ_2G^T - \prod_f C^T R_2^{-1} C \prod_f = 0 \tag{36}$$

TF of the KFMPC

The TF of the KFMPC is calculated with the use of K_{mpc} and K_f. The TF of the KFMPC is stated as:

$$K(s) = K_{mpc}(sI_n - A + BK_{mpc} + K_f C)^{-1} K_f \tag{37}$$

where $K(s)$ is the TF of KFMPC, I_n is an unitary matrix with dimension of $n \times n$, and n is the order of the system matrix A. The $K(s)$ is defined in matrix form [20]:

$$K(s) = \begin{bmatrix} A - BK_{mpc} - K_f C & K_f \\ -K_{mpc} & 0 \end{bmatrix} \tag{38}$$

The objective function j is the time integral of the transient and control energy. Therefore, it can be reduced by proper tuning of control variables Q_1 and R_1. The control variables R_1 and Q_1 govern the input $u(t)$ to the controller and the corresponding outputs of the system, respectively. The desired output is achieved through the controller by proper adjustment of the intensity of the Q_1 matrix. The uncontrolled process response of Fig. 2a–d indicates a larger impact of the imposed force $F(t)$ on the IPS outcomes. So, the states governing the IPS outcomes are assigned utmost weightage in the design of the controller. The estimation of the optimal values of the control variables

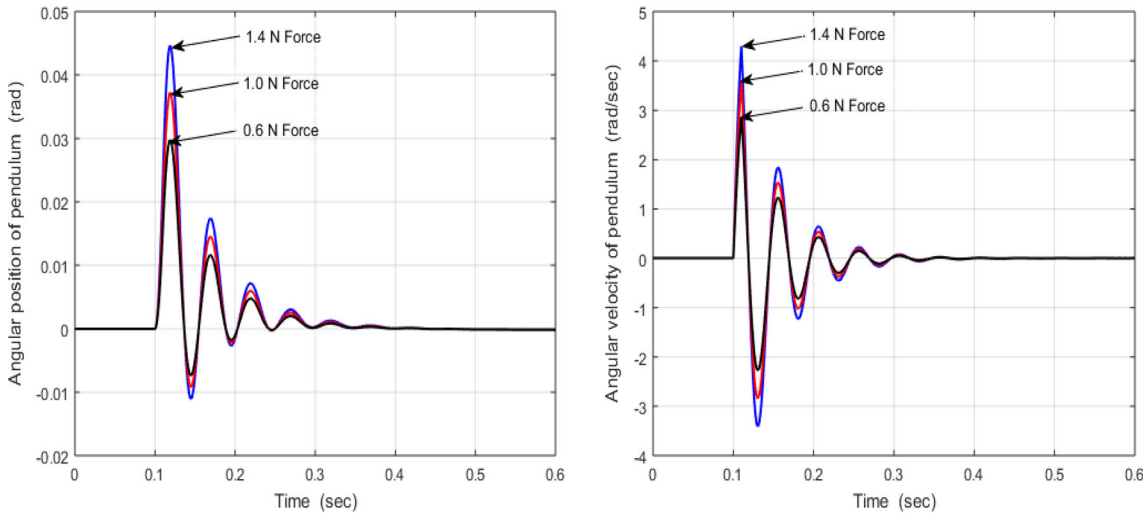

Fig. 7 **a** AP of the closed-loop IPS with variation of $F(t)$; **b** AV of the closed-loop IPS with variation of $F(t)$

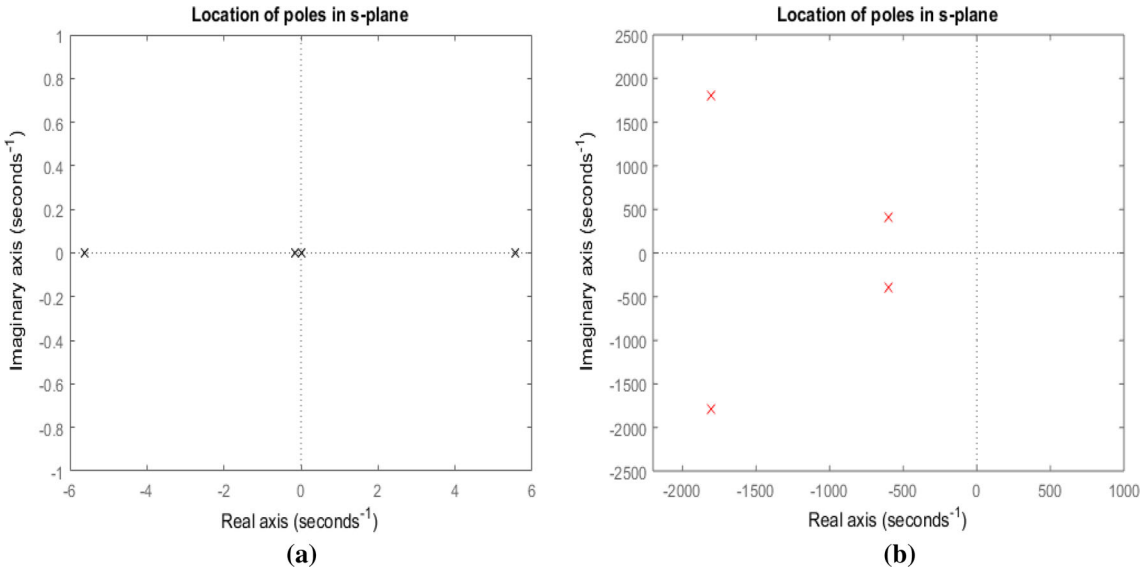

Fig. 8 **a** The open-loop IPS roots; **b** the closed-loop IPS roots

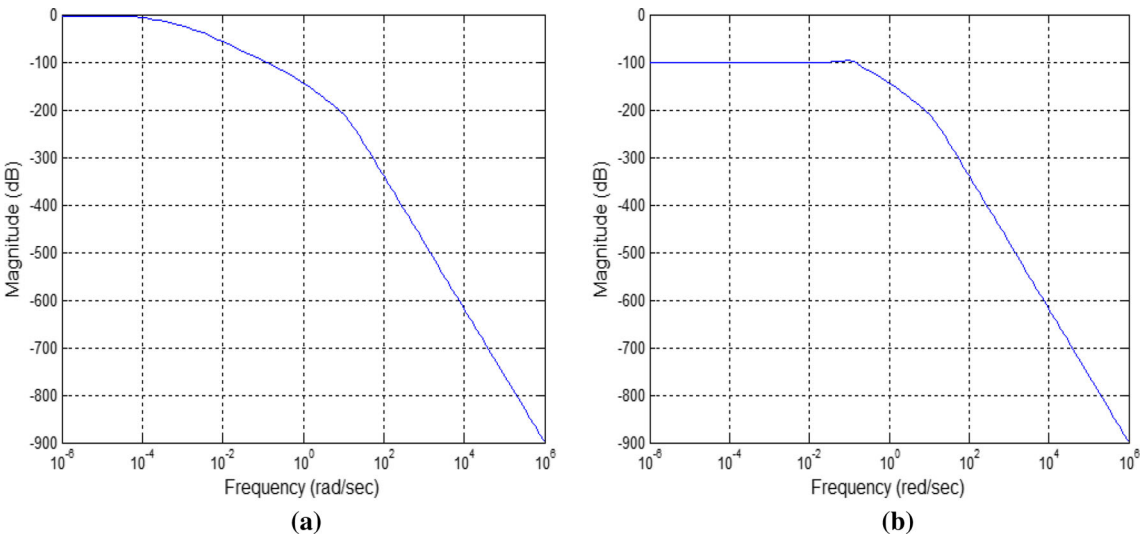

Fig. 9 **a** The Bode plot outcomes of the IPS; **b** the Bode plot outcomes of IPS with KFMPC

is evaluated with the assistance of MATLAB and aforementioned concept as detailed in Table 3. The KFMPC algorithm as a whole in a flowchart form is put in Fig. 4.

Outcomes and Deliberations

The activity of the IPS with KFMPC is depicted clearly in this division. The proposed strategy is contrasted with other well-known control approaches to validate its upgraded action.

System Activity with KFMPC

Right now, all outcomes of the IPS with KFMPC are inspected under various working conditions like deviation of $F(t)$. The closed-loop IPS outcomes with I N force are represented in Fig. 5a–d. The outcomes evidently specify the IPS achieves the AP and AV with zero value, and furthermore, cart accomplishes the steadiness location where it is completely consistent. To attain the updated system outcomes, the required $u(t)$ is caused by the KFMPC and reflected in Fig. 6.

Robustness of the KFMPC

Figure 7a, b exhibits the AP and AV of the IPS with KFMPC under the large variation of $F(t)$. The outcomes under large variation of $F(t)$ show the updated activities of the closed-loop IPS with KFMPC. For each situation, the IPS accomplishes zero angular position and zero angular

Table 4 Comparative study investigation associated with the AP in IPS

Controller	PID [5]	Fuzzy [7]	LQR [9]	$H\infty$ [15]	FSM [18]	BLQG [19]	KFMPC (Proposed)
Applied force (N)	1	1	1	1	1	1	1
t_s(sec)	2.8	3.0	3.2	1.5	1.6	0.4	0.36
O_{Peak}(rad)	0.1	0.226	0.081	0.107	0.042	0.041	0.037
U_{Peak}(rad)	0.01	0.087	0.02	0.045	0.151	0.01	0.008
Noise (%)	10	10	5	5	5	1	1
$e_{ss}(\%)$	0	0	0	0	0	0	0
Robustness	Less robust	Less robust	Less robust	Less robust	Less robust	Less robust	More robust
Stability	Less stable	Less stable	Less stable	Less stable	Less stable	Less stable	Absolute stable

velocity with less settling time. Thus, the IPS outcomes are very insensitive to $F(t)$. This prompts to robustness of a controller.

Stability Investigation

The IPS has 4 roots. But 1 root lies on the right adjacent of the frequency domain as reflected in Fig. 8a. It indicates the IPS is unstable. For upgrade of stability of the IPS, the KFMPC is formulated and executed. Accordingly, all roots of the system are pulled in the direction of the left side of the frequency domain as shown in Fig. 8b. Therefore, the IPS stability is upgraded because of the KFMPC.

Figure 9a, b shows the Bode plot outcomes of the open- and closed-loop IPS to confirm the stability circumstances. From these outcomes, a superior smoothness is observed which refers to the more steady-state stability of the closed-loop IPS (Fig. 9b) than the open-loop IPS (Fig. 9a). The operating frequency range is expanded in case of a closed-loop IPS with KFMPC than the open-loop IPS. This evidently specifies a quicker stable dynamics, and furthermore, IPS with KFMPC achieves zero angular position and velocity with less settling time. This approves improved stability during IPS action with KFMPC.

Comparative Study

The KFMPC is compared with other well-known control strategies to validate its upgraded performances. Figure 5a illuminates the influence of the $F(t)$ in the outcomes of the IPS with the KFMPC. Table 4 gives a near investigation with regard to t_s (sec), O_{Peak}(rad), U_{Peak}(rad), noise (%), and $e_{ss}(\%)$. The influence of the $F(t)$ in the outcomes of the IPS implementing well-known control methods is also exhibited in Table 4 with respect to the studies [5, 7, 9, 15, 18], and [19].

The outcomes of the IPS under the I N force are verified. The corresponding outcomes are exhibited for the different control methods together with KFMPC concerning control details such as O_{Peak}, U_{Peak}, and t_s. These outcomes imply the better controllability of the KFMPC. The outcomes additionally exhibit the noise suppression ability with more robustness of the KFMPC. Overall, it is observed from the above examination that the discoveries of the recommended KFMPC preferences are the higher accuracy and stability, more robustness, better ability to suppress noise, and better ability to monitor model uncertainty under different abnormal situations and large variation of applied force.

Conclusions

This study proposed a novel KFMPC for AP control in IPS within the stable range. For the formulation of the KFMPC, a 4th-order state-space model of the IPS is deliberated. In the KFMPC, the Kalman filter is employed to pull all the states toward the reference point to improve the control activity. The comparative outcomes obviously replicate that KFMPC is landed at preferred execution over the well-known control techniques regarding stability, accuracy, and robustness under different unusual situations and disturbances. The associated improved action of the proposed KFMPC as far as better accuracy, more robustness, improved stability, and better ability to suppress noise and model uncertainty validates its real-time implementation.

References

1. J. Iqbal, R.U. Islam, Z.A. Syed, A.K. Abdul, S.A. Ajwad, "Automating industrial tasks through mechatronic systems—A

review of robotics in industrial perspective. Tehnic ki vjesnik Tech. Gaz. **23**, 917–924 (2016)
2. S.A. Ajwad, N. Asim, R.U. Islam, J. Iqbal, Role and review of educational robotic platforms in preparing engineers for industry. Maejo Int. J. Sci. Technol. **11**, 17–34 (2017)
3. M. Bettayeb, C. Boussalem, R. Mansouri, U. Al-Saggaf, Stabilization of an inverted pendulum-cart system by fractional PI-state feedback. ISA Trans. **53**, 508–516 (2014). https://doi.org/10.1016/j.isatra.2013.11.014
4. J. Iqbal, M. Ullah, S.G. Khan, B. Khelifa, S. Ćukovic, Nonlinear control systems -A brief overview of historical and recent advances. Nonlinear Eng. **6**, 301–312 (2017). https://doi.org/10.1515/nleng-2016-0077
5. A. Ghosh, T. Krishnan, B. Subudhi, Brief paper –robust proportional-integral-derivative compensation of an inverted cart–pendulum system: An experimental study. IET Control Theory App. **6**(8), 1145–1152 (2012). https://doi.org/10.1049/iet-cta.2011.0251
6. C.Wang, G. Yin, C. Liu, and W. Fu, Design and simulation of inverted pendulum system based on the fractional PID controller, in *IEEE 11th Conference on Industrial Electronics and Applications (ICIEA)*, June 2016, pp. 1760–1764
7. M.E. Magana, F. Holzapfel, Fuzzy-logic control of an inverted pendulum with vision feedback. IEEE Trans. Educ. **41**(2), 165–170 (1998). https://doi.org/10.1109/13.669727
8. S. Ozana, M. Pies, Z. Slanina, and R. Hajovsky, Design and implementation of LQR controller for inverted pendulum by use of REX control system. in *IEEE International Conference on Circuit and Systems*, 2012, pp. 343–347
9. E.V. Kumar, J. Jerome, Robust LQR controller design for stabilizing and trajectory tracking of inverted pendulum. Procedia. Eng. **64**, 169–178 (2013). https://doi.org/10.1016/j.proeng.2013.09.088
10. L.B. Prasad, B. Tyagi, and H.O. Gupta, Modelling and simulation for optimal control of nonlinear inverted pendulum dynamical system using PID controller and LQR. in *2012 Sixth Asia Modelling Symposium (Ams)*, 2012, pp. 138–143
11. P. Frank, Evolving neurocontrollers for balancing an inverted pendulum. Netw Comput Neural Syst **9**(4), 495–511 (1998)
12. L. Deng, G. Shengxiang, The design for the controller of the linear inverted pendulum based on backstepping, in *Proceedings of 2011 International Conference on Electronic & Mechanical Engineering and Information Technology*, Vol. 6 (IEEE, 2011) pp. 2892–2895
13. M. Jörgl, K. Schlacher, H. Gattringer, Passivity based control of a cart with inverted pendulum, In *Applied Mechanics and Materials*, Vol. 332, pp. 339–344. Trans Tech Publications, 2013
14. T. Žilić, D. Pavković, D. Zorc, Modeling and control of a pneumatically actuated inverted pendulum. ISA Trans. **48**(3), 327–335 (2009)
15. P. Lambrecht, G. Vander, H-infinity control of an experimental inverted pendulum with dry friction. IEEE Contr. Syst. Mag. **13**(4), 44–50 (1988)
16. R.J. Wai, L.J. Chang, Adaptive stabilizing and tracking control for a nonlinear inverted-pendulum system via sliding-mode technique. IEEE Trans. Ind. Electron. **53**, 674–692 (2006). https://doi.org/10.1109/TIE.2006.870680
17. C.W. Tao, J. Taur, J. Chang, Adaptive fuzzy switched swing-up and sliding control for the double-pendulum and-cart system. IEEE Trans. Syst. Man Cybern. Part B Cybern. **40**(1), 241–252 (2010). https://doi.org/10.1109/TSMCB.2009.2025964
18. C.S. Chen, W.L. Chen, Robust adaptive sliding-mode control using fuzzy modeling for an inverted-pendulum system. IEEE Trans. Ind. Electron. **45**(2), 297–306 (1998). https://doi.org/10.1109/41.681229
19. A.K. Patra, S.S. Biswal, P.K. Rout, Backstepping linear quadratic gaussian controller design for balancing an inverted pendulum. IETE J. Res. **1**, 1–15 (2019)
20. W. Wang, Model predictive control design and implementation using MATLAB, ISBN 978-1-84882-330-3, (springer-verlag, London limited. 2009)
21. A.K. Patra, A.K. Mishra, P.K. Rout, Backstepping model predictive controller for blood glucose regulation in Type-I diabetes patient. IETE. J. Res. (2018). https://doi.org/10.1080/03772063.2018.1493404
22. A.K. Patra, P.K. Rout, Adaptive continuous-time model predictive controller for implantable insulin delivery system in Type I diabetic patient. Optim. Control Appl. Methods **38**(2), 184–204 (2017)
23. A.K. Patra, Adaptive sliding mode Gaussian controller for artificial pancreas in TIDM patient. J. Process Control **59**, 13–27 (2017)
24. A.K. Patra, Design of backstepping LQG controller for blood glucose regulation in type I diabetes patient. Int. J. Autom. Control **14**(4), 445–467 (2020)
25. A.K. Patra, Backstepping LQG controller design for stabilizing and trajectory tracking of vehicle suspension system. SN Appl. Sci. **2**(2), 190 (2020)
26. S. Karthick, K.S. Kumar, and S. Mohan, Relative analysis of controller effectiveness for vertical plane control of an autonomous underwater vehicle, in *OCEANS 2016-Shanghai*, (IEEE, 2016) pp. 1–6.
27. S. Irfan, A. Mehmood, M.T. Razzaq, J. Iqbal, Advanced sliding mode control techniques for inverted pendulum: modelling and simulation. Eng. Sci. Tech. Int. J. (2018). https://doi.org/10.1016/j.jestch.2018.06.010
28. G. Ronquillo-Lomeli, G.J. Ríos-Moreno, Nonlinear identification of inverted pendulum system using Volterra polynomials. Mech. Based Des. Struct. Mach. **44**(1), 5–15 (2016). https://doi.org/10.1080/15397734.2015.1028551
29. S. Kajita, F. Kanehiro, K. Kaneko, K. Fujiwara, Biped walking pattern generation by a simple three-dimensional inverted pendulum model. Adv. Robot. **17**(2), 131–147 (2003). https://doi.org/10.1163/156855303321165097
30. L. Canete, T. Takahashi, Modeling, analysis and compensation of disturbances during task execution of a wheeled inverted pendulum type assistant robot using a unified controller. Adv. Robot. **29**(22), 1453–1462 (2015). https://doi.org/10.1080/01691864.2015.1070106

Akshaya Kumar Patra

Publisher's Note Springer Nature remains neutral with regard to jurisdictional claims in published maps and institutional affiliations.